Near and Mid-infrared properties of known $z \geq 5$ Quasars

Nicholas P. Ross[1][⋆] and Nicholas J. G. Cross[1]

[1]*Institute for Astronomy, University of Edinburgh, Royal Observatory, Edinburgh, EH9 3HJ, United Kingdom*

18 February 2019

ABSTRACT

In this paper, we, for the first time since the discovery of $z \geq 5$ quasars, assemble all spectroscopically confirmed very high redshift quasars in one catalogue. In particular we present the near ($zZyYJHK_s$ and K) infrared and mid-infrared (WISE) properties of all 463 spectroscopically confirmed redshift $z \geq 5.00$ quasars. Using archival public WFCAM/UKIRT and VIRCAM/VISTA data we check for photometric variability in the near-infrared that might be expected from Super-Eddington accretion and find *blah*. We present a comprehensive series of colour-redshift and colour-colour plots and make inferences into the hot dust properties of the very high-redshift quasar population. Extrapolating the known quasar luminosity function we suggest that $x\%$ of the possibly detected $z \geq 5$ quasars in the current datasets have been discovered. All the data, analysis codes and plots used and generated here can be found at: github.com/d80b2t/VHzQ.

Key words: Astronomical data bases: surveys – Quasars: general – galaxies: evolution – galaxies: infrared.

1 INTRODUCTION

Very high redshift quasars (VHzQ; defined here to have redshifts $z \geq 5.00$) are excellent probes of the early Universe. This includes studies of the Epoch of Reionization for hydrogen (see e.g. Fan et al. 2006; Mortlock 2016, for reviews), the formation and build-up of supermassive black holes (e.g., Rees 1984; Wyithe & Loeb 2003; Volonteri 2010; Agarwal et al. 2016; Valiante et al. 2018; Latif et al. 2018; Wise et al. 2019) and early metal enrichment (see e.g., Simcoe et al. 2012; Chen et al. 2017; Bosman et al. 2017).

Super-critical accretion, where $\dot{M} > \dot{M}_{\rm Edd}$, is a viable mechanism to explain the high, potentially super-Eddington, luminosity and rapid growth of supermassive black holes in the early universe (e.g., Alexander & Natarajan 2014; Madau et al. 2014; Volonteri et al. 2015; Pezzulli et al. 2016; Lupi et al. 2016; Pezzulli et al. 2017; Takeo et al. 2018). Thus, one could expect VHzQs to potentially vary in luminosity as they go through phases of super-critical accretion. These signatures of photometric variability should be looked for, noting the rest-frame optical emission is redshifted into the observed near-infrared (NIR) at redshifts $z > 5$. Fortunately, data are now in place from deep, wide-field NIR instruments and surveys such as the Wide Field Camera (WFCAM) instrument on the United Kingdom Infra-Red Telescope (UKIRT) in the Northern Hemisphere

and the VISTA InfraRed CAMera (VIRCAM) on the Visible and Infrared Survey Telescope for Astronomy (VISTA) in the Southern Hemisphere, that are necessary for identifying VHzQs.

Quasars are known to be prodigious emitters of infrared emission, thought to be from the thermal emission of dust grains heated by continuum emission from the accretion disc (e.g., Richards et al. 2006; Leipski et al. 2014; Hill et al. 2014; Hickox et al. 2017). Observations in the mid-infrared, e.g. $\sim$3-30μm allow discrimination between AGN[1] and passive galaxies due to the 1.6μm "bump" entering the MIR at $z \approx 0.8 - 0.9$ (e.g., Wright et al. 1994; Sawicki 2002; Lacy et al. 2004; Stern et al. 2005; Richards et al. 2006; Timlin et al. 2016) as well as between AGN and star-forming galaxies due to the presence of Polycyclic Aromatic Hydrocarbon (PAHs) at $\lambda > 3\mu$m (e.g., Yan et al. 2007; Tielens 2008).

Jiang et al. (2006) and Jiang et al. (2010) report on the discovery of a quasar without hot-dust emission in a sample of 21 $z \approx 6$ quasars. Such apparently hot-dust-free quasars have no counterparts at low redshift. Moreover, those authors demonstrate that the hot-dust abundance in the 21 quasars builds up in tandem with the growth of the central

---

⋆ Corresponding Author: npross@roe.ac.uk

[1] Historically, "quasars" and "Active Galactic Nuclei (AGN)" have described different luminosity/classes of objects. In recognition of the fact that both terms describe accreting supermassive black holes, we use these terms interchangeably, with a preference for quasar, since we are generally in the higher-L regime (e.g. Haardt et al. 2016).

black hole. But understanding how dust first forms and appears in the central engine remains an open question (Wang et al. 2008, 2011).

WISE mapped the sky in 4 passbands, in bands centered at wavelengths of 3.4, 4.6, 12, and $23\mu m$. The all sky 'ALLWISE' catalogue release, contains nearly 750 million detections at high-significance[2], of which over 4.5M AGN candidates have been identified with 90% reliability (Assef et al. 2018). Blain et al. (2013) presented WISE mid-infrared (MIR) detections of 17 (55%) of the then known 31 quasars at $z > 6$. However, Blain et al. (2013) was compiled with the WISE 'All-Sky' data release, as opposed to the superior AllWISE catalogues. That sample only examined the 31 known $z > 6$ quasars; our sample has 170 objects with redshift $z \geq 6.00$ (with x detected in WISE **NPR to double check!!**). Bañados et al. (2016) reports WISE W1, W2, W3 and W4 magnitudes for the Panoramic Survey Telescope and Rapid Response System 1 (Pan-STARRS1, PS1; Kaiser et al. 2002, 2010), but with no further investigation into the reddest WISE waveband for the VHzQs.

Critically, we now have available to us new W1 and W2 photometry from the 'unWISE Source Catalog' (Schlafly & Meisner 2018), a WISE-selected catalogue that is based on significantly deeper imaging and has a more extensive modeling of crowded regions than the ALLWISE release. For the first time in a catalogue, unWISE takes advantage of the ongoing mid-IR Near-Earth Object Wide-Field Infrared Survey Explorer Reactivation mission (NEOWISE-R; Mainzer et al. 2014), and achieves depths ∼0.7 mag deeper than ALL-WISE (in W1/2). This additional depth is a significant advantage in the detection and study of VHzQs in the 3-5 micron regime.

Here we present for the first time the combined near-infrared properites (from UKIRT and VIRCAM) and the new mid-infrared unWISE for all the spectroscopically known $z \geq 5.00$ quasars. Our motivations are numerous and include: *(i)* establishing the first complete catalogue of $z > 5.00$ quasars since the pioneering work from SDSS; *(ii)* utilizing all the WFCAM and VISTA near-infrared photometry available for the quasars; *(iii)* making the first study of near- and mid-IR variability of the VHzQ population and *(iv)* establishing the photometric properties for upcoming surveys and telescopes including the Large Synoptic Survey Telescope (LSST)[3], ESA *Euclid*[4] and the *James Webb Space Telescope* (JWST)[5,6,7,8]. We chose redshift $z = 5.00$ as our lower redshift limit due to a combination of garnishing a large sample, adequately spanning physical properties (e.g. luminosity, age of the Universe) and to highlight the parts of $L - z$ parameter space where $z > 5$ quasars still wait to be discovered.

This paper is organized as follows. In Section 2, we present the assembled list of the 463 $z \geq 5.00$ VHzQs that we have compiled. We then give a high-level overview of the photometric surveys and datasets we use and present the
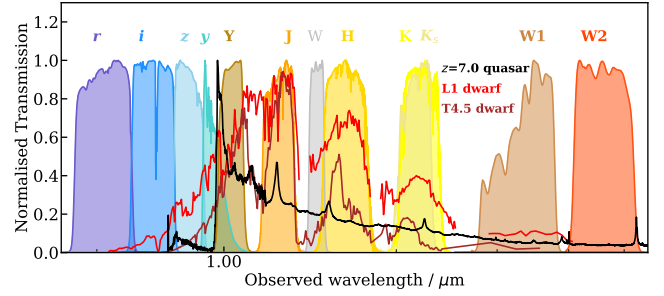
Figure 1. The spectral bands used by different survey telescopes and that are relevant here. The *grizy* filters are from the Pan-STARRS survey. The *JHK* are from UKIRT/WFCAM, while K_s is a VISTA/VIRCAM filter. The The narrow W-band centered at $\lambda \approx 14,500$Å is a CFHT/Wircam filter. [NJC: Do we use the W-band anywhere?] The WISE passbands W1-4 are also presented. The quasar spectrum is a composite based on Vanden Berk et al. (2001) and Bañados et al. (2016). The L and T dwarf spectra are from Cushing et al. (2006).

photometry of the VHzQs. In Section 3 we ... and In Section 4 we ... We conclude in Section 5 and present all the necessary details to obtain our dataset in the Appendices.

We present all our photometry and magnitudes on the AB zero-point system (Oke & Gunn 1983; Fukugita et al. 1996). This includes the near-infrared, as well as the mid-infrared magnitudes. Appendix A gives the AB to Vega transforms for a wide range of optical, NIR and MIR filters. We use a flat ΛCDM cosmology with $H0 = 67.7$ km s−1 Mpc1, $\Omega_M = 0.307$, and $\Omega_\Lambda = 0.693$ (Planck Collaboration et al. 2016) to be consistent with Bañados et al. (2016) and all logarithms are to the base 10.

2   METHOD AND DATA

Quasars are generally identified by photometric selection followed by spectroscopic confirmation. Here, we reverse this method obtaining first a list of spectroscopic quasars and then obtain photometric information.

We have compiled a list of 463 quasars with redshifts $z \geq 5.00$. We use all the $z \geq 5.00$ quasars that have been discovered, spectroscopically confirmed and published as of 2018-Dec-31. We then obtain optical, near-infrared and mid-infrared photometry for the spectral dataset. The optical data comes from the Panoramic Survey Telescope and Rapid Response System (Pan-STARRS) survey (Chambers et al. 2016). The near-infrared data comes from two sources: first, the WFCAM (Casali et al. 2007) on the UKIRT, primarly, but not exclusively, as part of the UKIRT Infrared Deep Sky Survey (UKIDSS; Lawrence et al. 2007). And second, data from the VIRCAM on the VISTA (Emerson et al. 2006; Dalton et al. 2006). The mid-infrared, $\lambda = 3 - 30\mu m$ wavelength data is from the the Wide-Field Infrared Survey Explorer (WISE; Wright et al. 2010; Cutri 2013) mission. For reference, Figure 1 displays the wavelength and normalised transmission of the filters in question.

2.1   Spectroscopy

We compile the list of all known, spectroscopically confirmed quasars from the literature. This list was complied from a

Figure 2. The redshift distribution $N(z)$ of the VHzQ sample. The bins are $\delta - z = 0.075$ in width.

Survey	# VHzQs	(%)	Survey reference
ATLAS	4	(0.86)	Shanks et al. (2015)
CFHQS	20	(4.32)	Willott et al. (2007)
DELS	16	(3.46)	Dey et al. (2018)
ELAIS	1	(0.22)	Väisänen et al. (2000)
FIRST	1	(0.22)	Becker et al. (1995)
HSC	8	(1.73)	Miyazaki et al. (2018)
IMS	5	(1.08)	Kim et al. (2015)
MMT	12	(2.59)	McGreer et al. (2013)
NDWFS	1	(0.22)	Jannuzi & Dey (1999)
PSO	83	(17.93)	Kaiser et al. (2002, 2010)
RD	1	(0.22)	Mahabal et al. (2005)
SDSS	170	(36.72)	Stoughton et al. (2002)
SDWISE[b]	27	(5.83)	Wang et al. (2016)
SHELLQs	55	(11.88)	Matsuoka et al. (2016)
SUV[c]	20	(4.32)	Yang et al. (2017)
UHS	1	(0.22)	Wang et al. (2017)
ULAS	10	(2.16)	Lawrence et al. (2007)
VDES[d]	17	(3.67)	Reed et al. (2017)
VHS	1	(0.22)	Wang et al. (2018a)
VIK	9	(1.94)	Edge et al. (2013)
VIMOS	1	(0.22)	Le Fèvre et al. (2003)

Table 1. The source and number of the VHzQ, with the key survey reference also given. Recent survey name and acronyms include: [a]DESI Legacy Imaging Survey; [b]SDWISE = SDSS+WISE; [a]SUV = SDSS-ULAS/VHS; [c]VDES = VHS/VIKING+DES;

$z \geq$	Age / Myr	No. of objects
7.50	700	1
7.00	767	4
6.78	800	14
6.50	845	40
6.19	900	86
6.00	937	170
5.70	1000	267
5.00	1180	463

Table 2. The number of objects at or above a given redshift. The age of the Universe in megayears is also given.

range of surveys and papers. Specifically, we use data from: Bañados et al. (2014, 2016, 2018), Becker et al. (2015), Calura et al. (2014), Carilli et al. (2007, 2010), Carnall et al. (2015), Cool et al. (2006), De Rosa et al. (2011), Fan et al. (2000, 2001, 2003, 2004, 2006, 2018), Goto (2006), Ikeda et al. (2017), Jiang et al. (2008, 2009, 2015); **?**, Kashikawa et al. (2015), Koptelova et al. (2017), Kim et al. (2015, 2018), Kurk et al. (2007, 2009), Leipski et al. (2014), Mahabal et al. (2005), Matsuoka et al. (2016, 2018a,b), Mazzucchelli et al. (2017), Morganson et al. (2012), Mortlock et al. (2009, 2011), McGreer et al. (2006, 2013), Reed et al. (2015, 2017), Stern et al. (2007), Tang et al. (2017), Venemans et al. (2007, 2012, 2013, 2015b,a, 2016), Wang et al. (2016, 2017, 2018b,a), Willott et al. (2007, 2009, 2010, 2013, 2015), Wu et al. (2015) Yang et al. (2018b,a) and Zeimann et al. (2011).

Most of these objects are easily identified by their broad Lyα emission line, N V emission and characteristic shape blueward of 1215Å in the rest-frame. As we shall see, some of the recently discovered objects are close to the galaxy luminosity function characteristic luminosity M^*, and some have relatively weak or maybe even completely absorbed Lyα (e.g. Figures 7 and 10 in Bañados et al. 2016). We leave aside detailed investigation and discussion into spectral features and line strengths, and take as given the published spectra and redshift identifications.

The breakdown of how many VHzQ each survey reports is given in Table 1. The Sloan Digital Sky Survey (SDSS) and the Pan-STARRS1 (PS1; PSO in Table 1) survey and alone identified over half (54.6%) of the VHzQ population. Data from the Hyper Suprime-Cam (HSC) on the Subaru telecope is responsible for 13.6% of our dataset (HSC+SHELLQs in Table 1). The combination of surveys is also vital for identifying VHzQs. The UKIDSS Large Area Survey (ULAS) on its own, or in combination with other surveys is responsible for 6.5% of the sample (SUV+ULAS) including the highest-z object. Where more than one survey is used for the high-redshift identification (e.g. via shorter-band veto and longer wavelength detection) we follow the discovery paper naming convention.

The redshifts for the VHzQs generally come from the measurement of broad UV/optical emission lines. There are far infra-red emission lines e.g. C II 158 micron available for several objects, but at the level of our current analysis broadline redshifts are sufficient.

The number of objects at or above various redshifts, along with the corresponding age of the Universe is given in Table 2.

The $N(z)$ redshift histogram is given for the sample in Figure 2. We split the contribution up by survey. For clarity we show the individual surveys of SDSS, PS1, HSC, the ULAS detection, and tally the remaining surveys together ("various"). In Section **??** we discuss the form of the $N(z)$ as well as the coverage of the luminosity-redshift $L - z$ plane.

2.2 Optical Photometry

We query the Panoramic Survey Telescope and Rapid Response System (Pan-STARRS)[9] Data Release 1 (DR1) Catalog Archive Server Jobs System (CasJobs) service at mastweb.stsci.edu/ps1casjobs/. The Pan-STARRS1 (PS1) survey observed the 30,000 deg^2 of sky north of declination $\delta = -30$ degrees in the five *grizy* filters. PS1 is the first part of Pan-STARRS to be completed and is the basis for the DR1. Chambers et al. (2016), Magnier et al. (2016c),

[9] https://outerspace.stsci.edu/display/PANSTARRS

Waters et al. (2016), Magnier et al. (2016a), Magnier et al. (2016b) and Flewelling et al. (2016) describe the instrument, survey, and data analyses. The principal science product of the PS1 survey is the catalog accessible through the CasJobs interface.

We query and return the mean PSF magnitudes from the *grizy* filters (MeanPSFMag) which are in the AB system for our 463 VH*z*Q sample. Our SQL and links to the main PS1 DR1 tables are given in Appendix B.

2.3 Near-infrared photometry

The near-infrared data in this paper comes from the Wide Field Astronomy Unit's (WFAU) Science Archives for UKIRT-WFCAM, the WFCAM Science Archive (WSA; Hambly et al. 2008) and VISTA-VIRCAM, the VISTA Science Archive (VSA; Cross et al. 2012). These archives were developed for the VISTA Data Flow System (VDFS Emerson et al. 2004).

We access both the WSA and the VSA and include all non-proprietary WFCAM data, which covers all public surveys and PI projects from Semester 05A to 2017-Jan-01, and all non-proprietary VISTA data, which covers all public surveys and PI projects from science verification on 2009-Oct-15 to 2016-Apr-01.

Here we are not just quering the WSA or VSA data tables. We are taking a list of objects (positions) are performing matched aperature ("forced") photometry on the NIR imaging data. As such, we generate a set of tables that are different in subtle ways to the regular "Detection" tables. The two most important tables for our needs are the [w/v]serv1000MapRemeasurement and [w/v]serv1000MapRemeasAver.

We produce and provide a two new databases with all the necessary quantaties and measurements to fully reproduce our tables, figures and results herein. Morever, these databases report considerably more information than we report here. Full documentation can be found at the WSA Schema Browser and the VSA Schema Browser.

2.3.1 Averaging matched photometry

The data was processed using a matched-aperture photometry method where flux is measured at the spectroscopic position of the quasar, without necessarily knowing if there is a formal detection in the NIR photometry beforehand. The matched-aperture pipeline is discussed in Cross et al. (2013) and with fuller details to appear in a forthcoming paper (Cross et al., 2019, in prep).

We query the WSA and VSA performing matched-aperature photometry at the positions of our 463 VH*z*Qs. This database is world-readable and we give the full receipe and relevant SQL queries for accessing both databases in Appendix D as well as online.

The photometry in a single epoch image often has low signal-to-noise. The advantage of matched aperture photometry on quasars is that co-adding is relatively simple if each epoch is taken in the same aperture and the aperture photometry has been corrected to total. Indeed, the standard aperture corrections work well for point sources. Coadding using the matched-aperature photometry, where the individual epochs are taken from multiple projects with different

pointings and orientations, should help with issues such as scattered light, pixel distortion and aperture corrections.

We average the aperture corrected calibrated fluxes (e.g. **aperJky3**), and then convert to magnitudes. Since we do not have a deep image for each set of averages, we cannot calculate non-aperture corrected values, so the photometry is only appropriate for point-sources.

$$\bar{F} = \frac{\sum_i^N (w_i\, F_i)}{\sum_i^N w_i} \tag{1}$$

where F_i is the ith epoch measurement of a parameter to be averaged such as the aperture corrected calibrated flux in a $1''$ aperture (**aperJky3**) and $\bar{F}$ is the weighted mean average of this parameter. The weight for each epoch $w_i = 1/(\sigma_F)^2$ if the epoch is included and $w_i = 0$ if an epoch is excluded for quality control purposes.

We calculate a set of averaged catalogues, for each pointing and filter, based on the requirements in RequiredMapAverages, in these cases over time spans of 7, 14, 30, 91, 183 days, 365 days, 730 days, over 10 epochs and over all epochs. The averaging process starts at the first epoch and works onwards from there. Again, we present these measurements in the new SQL tables.

We detect 304 unique quasars in the WFCAM WSA database, 203 quasars are detected in the VISTA VSA database with 114 objects in common with both WFCAM and VISTA data. We give the necessary SQL queries syntax in Appendix D.

2.4 MIR data

The MIR data for this study comes from the Wide-field Infrared Survey Explorer (WISE) mission, and we utlize data from the WISE cryogenic and NEOWISE (Mainzer et al. 2011 ApJ, 731, 53) post-cryogenic survey phases.

We use data from the the beginning of the WISE mission (2010 January; Wright et al. 2010) through the fourth-year of NEOWISE-R operations (Mainzer et al. 2011, 2017 December;). More specifically, we utilise the recently released "unWISE Catalog" **?**. The unWISE effort[10] is the unblurred coadds of the WISE imaging using the AllWISE and NEOWISE-R stacked data (Lang 2014; Meisner et al. 2018a,b).

All fluxes in the unWISE catalog are reported there are in "Vega nanoMaggies", with the Vega magnitude of a source is given by $m_{\text{Vega}} = 22.52.5\log(f)$, where f is the source flux. The absolute calibration for unWISE is ultimately inherited from AllWISE through the calibration of **?**. This inheritance depends on details of the PSF normalization at large radii, which is uncertain. Subtracting 4 mmag from the unWISE W1, and 32 mmag from unWISE W2 fluxes improves the agreement between unWISE and AllWISE fluxes.

Thus to convert unWISE Vega magnitudes onto the AB system, we have

$$\begin{aligned}
\text{W1}_{\text{AB,unWISE}} &= 22.5 - 2.5\log(f_{\text{W1}}) - 0.004 + 2.699 \\
\text{W2}_{\text{AB,unWISE}} &= 22.5 - 2.5\log(f_{\text{W2}}) - 0.032 + 3.339
\end{aligned}$$

---

[10] http://unwise.me/

those two numbers are how far our flux measurements differed on average from the AllWISE flux estimates at high Galactic latitudes. These tweaks will move you closer to the AllWISE absolute calibration, which we haven't tried to improve upon.

For the our MIR variability investigations, we do not use the unWISE coadds, but instead use the AllWISE catalogue and the NEOWISE 2018 Data Release. NEOWISE 2018 makes available the 3.4 and 4.6 m (W1 and W2) single-exposure images and extracted source information that was acquired between 2016 December 13 and 2017 December 13 UTC, which was the fourth year of survey operations of the Near-Earth Object Wide-field Infrared Survey Explorer Reactivation Mission (NEOWISE; Mainzer et al. 2014, ApJ, 792, 30). The fourth year NEOWISE data products are concatenated with those from the first three years into a single archive.

The WISE scan pattern leads to coverage of the full-sky approximately once every six months (a "sky pass"), but the satellite was placed in hibernation in 2011 February and then reactivated in 2013 October. Hence, our light curves have a cadence of 6 months with a 32 month sampling gap.

Tables 3, **??** and **??**, represent the culmination of this effort, and we now describe the assembly of their contents in more detail.

3 RESULTS

Having collated the sample of 463 VHzQs, and obtained their optical, near- and mid-infrared photometry we report here the various photometric properites of the quasars.

First, we will concentrate on detection rate in the infrared, go on to report on the color-redshift and color-color properties of our sample and then report on how the current sample populates the luminosity-redshift Lz-plane.

3.1 Detection Rates in the NIR

Table 4 gives the detection rates for the VHzQs in the NIR $YJHK/K_s$-bands. The first thing to note is that the coverage of the NIR surveys for example from the UKIDSS LAS and VISTA VHS, does not overlap the full area for where the VHzQs are detected.

3.1.1 Comparing WFCAM and VISTA

There are 114 overlapping QSOs between WFCAM and VISTA. Using the `VegaToAB` value[11] to put these objects on the same AB system, and for each object compared the two measurements. First, the calculated weighted average (calibrated flux) in each filter of both and calculated the ratio and difference between each measurement and the average. Then for each filter we calculated the weighted average of the differences (in mag) for each instrument to see if there were significant offsets. The results are given in Table 5. The only filter with a significant offset is the Y-band. All of the VISTA averages are negative and all of the WFCAM ones
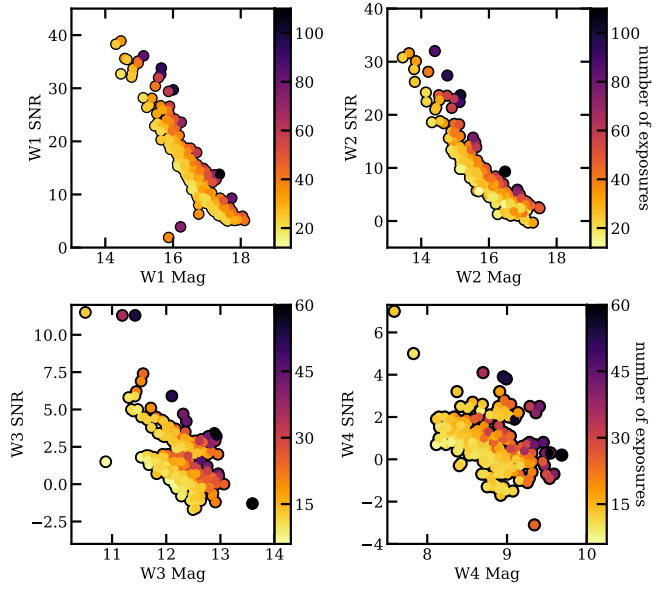
---

[11] What is this exactly??

Figure 3. WISE W1/2/3/4 magnitude against signal-to-noise, colour coded by w$x$cov the mean coverage depth, in each corresponding band.

are positive. The Ks versus K band may be slightly dodgy, given the different shapes of the filters.

3.2 Detection Rates in the MIR

Unlike the NIR coverage, the WISE satellite and mission performed an all-sky survey, so the location of evey VHzQ in our dataset is covered. However, the depth of the WISE ALLWISE survey depends heavily on sky location, with locations near the Ecliptic Poles having the highest number of exposures.

Before reporting on the detection rates, we investigate this effect. Figure 4 shows the WISE magnitude versus signal-to-noise, colour coded by `wxcov` the mean coverage depth, in each corresponding band. In the two shorter bands W1/2 we see the clear and expected trend for brighter objects to have larger SNR, and also for the higher signal to noise for objects with more exposures at a given magnitude. The behaviour for the W3/4 bands is different, with two populations clearly evident in W3 and although a bit more mixed, also in W4. With the suggested split at SNR> 2, and no obvious R.A./Declination dependence seen, this behaviour is explained by the fact that there are non-detectiopns in W3/4 for objects (with high W1/2 SNR) that are reported in the ALLWISE catalogue.

For the 278 VHzQ with coverage detections, the mean number of exposures for the W1/2 bands is 32.0 and 31.5, respectively, with a minimum number of exposures 17 and 12, and the maximum number or exposures being 114 (for both bands). For the W3/4 filters, the corresponding mean, minimum and maximum exposure are 17.4 and 17.5, 5.8 and 6.8 and 69 (for both bands). These values are direclty from the `wxcov` enteries in the WISE ALLWISE catalogue.

Table 7 gives the detection rates for the VHzQs in the MIR WISE W1-4 bands.

Blain et al. (2013)

na	desig	ra_hms	dec_dms	ra	dec	redshift	mag	M1450	ref
PSO	J000.3401+26.8358	00:01:21.63	+26:50:09.17	0.340113	+26.83588	5.75	19.52	-27.16	1/1/1
SDSS	J0002+2550	00:02:39.39	+25:50:34.80	0.664117	+25.84304	5.82	19.39	-27.31	5/22/1
SDSS	J0005-0006	00:05:52.34	-00:06:55.80	1.468083	-00.11549	5.85	20.98	-25.73	5/12/1
PSO	J002.1073-06.4345	00:08:25.77	-06:26:04.60	2.107390	-06.43456	5.93	20.41	-26.32	1;43/1/1
SDWISE	J0008+3616	00:08:51.43	+36:16:13.49	2.214292	+36.27041	5.17	19.12	-27.34	Wang2016
PSO	J002.3786+32.8702	00:09:30.89	+32:52:12.94	2.378702	+32.87026	6.1	21.13	-25.65	1/1/1
SDSS	J0017-1000	00:17:14.68	-10:00:55.4	4.311166	-10.01540	5.011	99.99	-99.99	DR7_W16
PSO	J004.3936+17.0862	00:17:34.47	+17:05:10.70	4.393614	+17.08631	5.8	20.69	-26.01	1/1/1
PSO	J004.8140-24.2991	00:19:15.38	-24:17:56.98	4.814080	-24.29920	5.68	19.43	-27.24	1/1/1
VDES	J0020-3653	00:20:31.46	-36:53:41.8	5.131124	-36.89495	6.9	99.99	-99.99	DES-VHS_inprep

Table 3. All 424 $z \geq 5.00$ quasars that have been spectroscopically confirmed as of 2018 June. The first ten objects are given here as guidance to the format of the data table. The full table can be found online.

Selection	number detected (%)
Any band ($ZYJHK/K_s$	394 (92.9)
Z-band	72 (17.0)
Y-band	249 (58.7)
J-band	391 (92.2)
H-band	258 (60.8)
K or Ks-band	297 ( )

Table 4. Detection rate of VHzQs in the near-infrared.

abs(VIRCAM - WFCAM)	millimags	no. of objects
Z	19.3	2
Y	66.2	48
J	3.2	105
H	19.3	89
K_s/K	12.7	93

Table 5. Comparing the magnitudes in different WF-CAM/UKIRT and VIRCAM/VISTA near-infrared bands.

Selection	number detected (%)
W1 SNR > 2.0	275 (64.9)
W2 SNR > 2.0	255 (60.1)
W1 ∧ W2 SNR > 2.0	
W3 SNR > 2.0	99 (23.3)
W4 SNR > 2.0	29 (6.8)
Any W1/2/3/4 SNR > 2.0	
W1/2 SNR < 2.0 ∧ W3 SNR > 2.0	

Table 6.

Selection	number detected (% of full specrta)
From "Source", "Rejects",	245, 40 (67.2)
W1 SNR > 2.0	279 (65.8)
W2 SNR > 2.0	258 (60.8)
W1 ∧ W2 SNR > 2.0	253 (59.7)
W3 SNR > 2.0	97 (22.9)
W4 SNR > 2.0	33 (7.8)
W1/2 SNR < 2.0 ∧ W3 SNR > 2.0	3 (0.7)

Table 7. Data from the AllWISE Source Catalog and AllWISE Reject Table, from the NASA/IPAC Infrared Science Archive
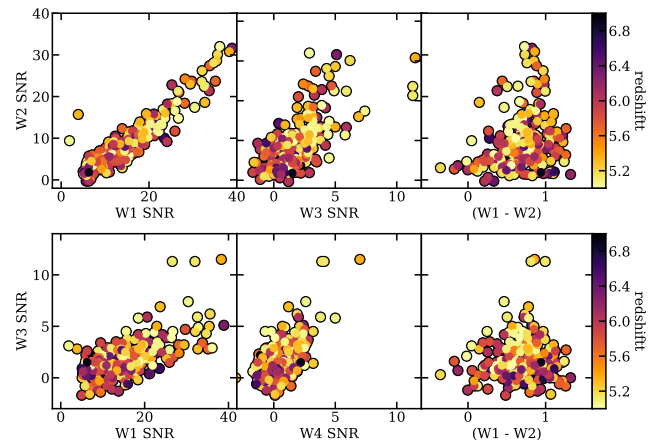

Figure 4. WISE signal-to-noise measures for the four bands, as well as for (W1-W2) colour. The points are colour coded by redshift.

Recently, Assef et al. (2018) released two large catalogues of AGN candidates identified across 30,000 deg^2 of extragalactic sky from the WISE AllWISE Data Release. The "R90" catalogue, is contains 4.5M AGN candidates at 90% reliability (and $\approx$150 AGN candidates per deg^2) while the "C75" catalog consists of 20.9M AGN candidates at 75% completeness (and ($\approx$700 AGN candidates per deg^2). Cross-matching out catalogue of 463 VHzQs with these catalogues, produces 42 matches with the R90 sample and 98 matches with the C75 sample. Both catalogues unsurprisingly match to the ultraluminous quasar SDSS J0100+2802 (Wu et al. 2015) while the C75, but not the R90 catalogue mathes to ULAS J1120+0641 (Mortlock et al. 2011). Neither catalogue matches J1342+0928 (Bañados et al. 2018).

Very High-z Quasars Detected in WISE W3 and W4.

3.3 Variability

VHzQs, if accreting at, or above the Eddington Limit, might well have have large values of changing mass accretion rate, $\ddot{m}_{\rm accr}$. A consequence of this would be that these quasar exhibit signs of variability, most likely showing up in their UV/optical rest-frame spectra. We look for evidence of this variability signature in the NIR and MIR light-curves of the VHzQs. As a guide, C IV enters the Y-band at redshift z=5.32 and exits at z=5.99, and enters the J-band at red-
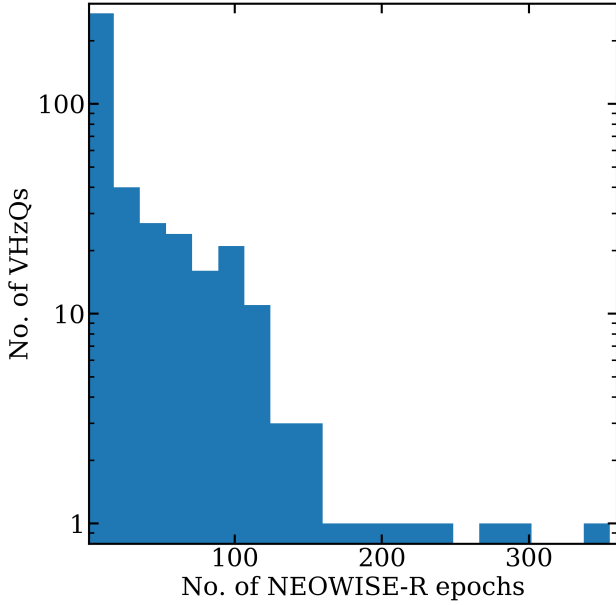
Figure 5. Histogram showing the number of NEOWISE-R epochs and detections there are for each VHzQ.

Figure 6. Here we show the MIR NEOWISE-R for J0100+2802 (Wu et al. 2015), J0224-4711 and J1626+2751. Red points are the W1 band; cyan points the W2 band.

shift $z = 6.55$ and exits at $z=7.57$. Mg II enters the H-band at redshift $z = 4.33$ and exits at $z = 5.37$ and enters the K-band at redshift $z = 6.25$ and exits at 7.50.

Using the extended datasets described in Section 2.3 and **??**, we

Figure 5 gives the number of NEOWISE-R epochs and detections there are for each VHzQ, while Figure **??** presents three examples of the MIR lightcurves and associated colour changes. Here we show J0100+2802 (Wu et al. 2015), J0224-4711 and J1626+2751. **NJC: What about NIR lightcurves / combined light-curves**

3.4 Colours

Currently, very high-redshift quasars are identified by their morphology, flux and colours in optical and infrared imaging data Fan (1999); Mortlock et al. (2012) Quasars are generally selected to be point sources, but be outliers from the stellar locus in colour space. For VHzQs, the main technique is to look for objects with extreme optical-to-near-infrared colours The lack of proper motion can also help identified quasars (e.g. Lang et al. 2009).

Figure 7 presents the optical colour-redshift trends for Late Type M/L/T dwarfs and the VHzQs.

3.5 L-z Plane

Having obtained an as-near-to-homogenous set of photometry as we can, we are now in a position to calculate the Absolute Magnitudes of the VHzQ sample and in particulare the absolute magnitude at rest-frame 1450Å , M_{1450}, which is a key physical quantity and goes directly towards the quasar luminosity function and thus the reionization of hydrogen calculation.

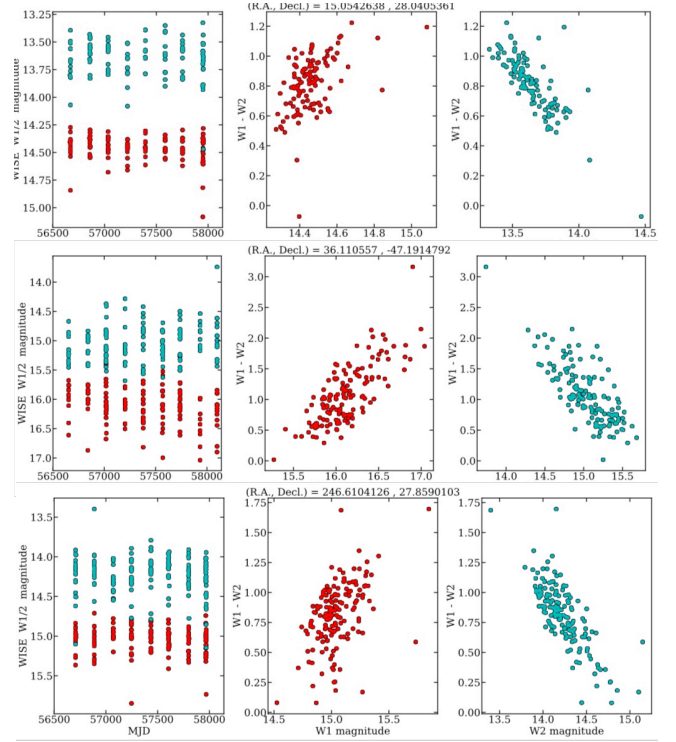We calculate the Distance Modulus in the normal fashion,

$$m_{1450} - M_{1450} = 5 \log \left(\frac{D_{\mathrm{L}}(z)}{\mathrm{Mpc}} \right) + 25 + K_{\mathrm{corr}}(X, z) \quad (2)$$

where m_{1450} is the apparent magnitude at 1450Å , $D_{\mathrm{L}}(z)$ is the luminosity distance and $K_{\mathrm{corr}}(X, z)$ is the K-correction which corrects for the effects of redshifting of the bandpass and the spectrum.

The m_{1450} apparent magnitude is derived from the $z-$, $y/Y-$ or $J-$band photometery.

The Pan-STARSS1 z_{PS1} and y_{PS1}-bands approximatley sample the redshift ranges $4.53 \leq z \leq 5.45$ and $5.28 \leq z \leq 6.47$, respectively for 1450Å' emission, while the VIRCAM $Y_{\mathrm{VIRCAM}}-$ and J_{VIRCAM}-bands cover $5.50 \leq z \leq 6.57$ and $7.06 \leq z \leq 8.16$.

Ross et al. (2013) has a detailed discussion of the K-correction (see that papers' Appendix B). The key result in that paper is, if quasars are described as having a power-law slope, α^{ν} in spectral flux density, i.e., $f_{\nu}(\nu) \propto \nu^{\alpha_{\nu}}$ (as is conventional) then

$$K_{\mathrm{corr}}(z) = -2.5(1 + \alpha_{\nu}) \log[1 + z]. \quad (3)$$

Here the $[-2.5 \log(1+z)]$ term corrects for the effective narrowing of the filter width with redshift, (the "bandpass correction") and the $[-2.5\alpha^{\nu} \log(1+z)]$ term takes into account the spectral index correction. The bandpass correction is approximately ≈ -1.945 at redshift $z = 5$ decreasing to -2.32 at redshift $z = 7.50$.
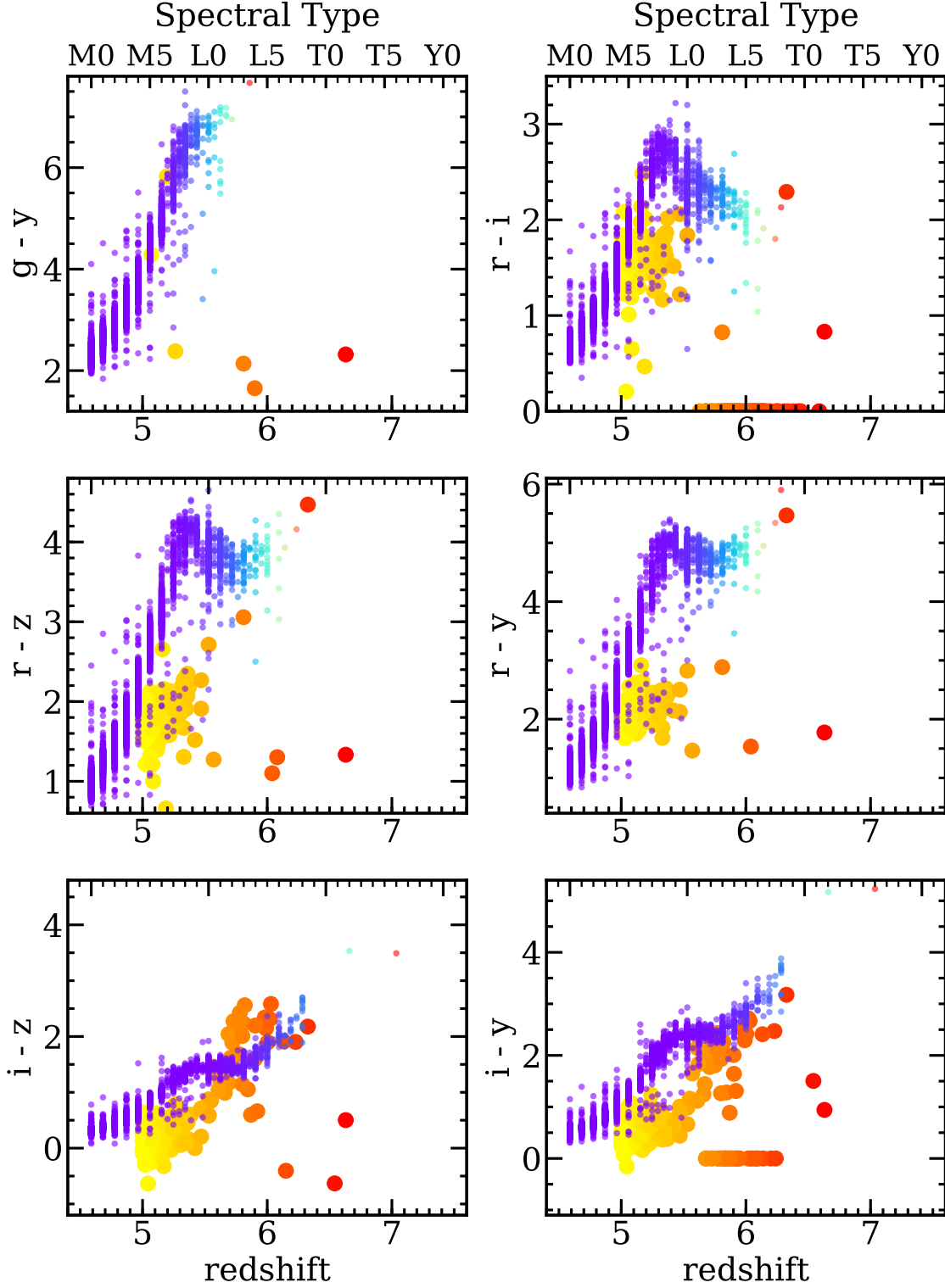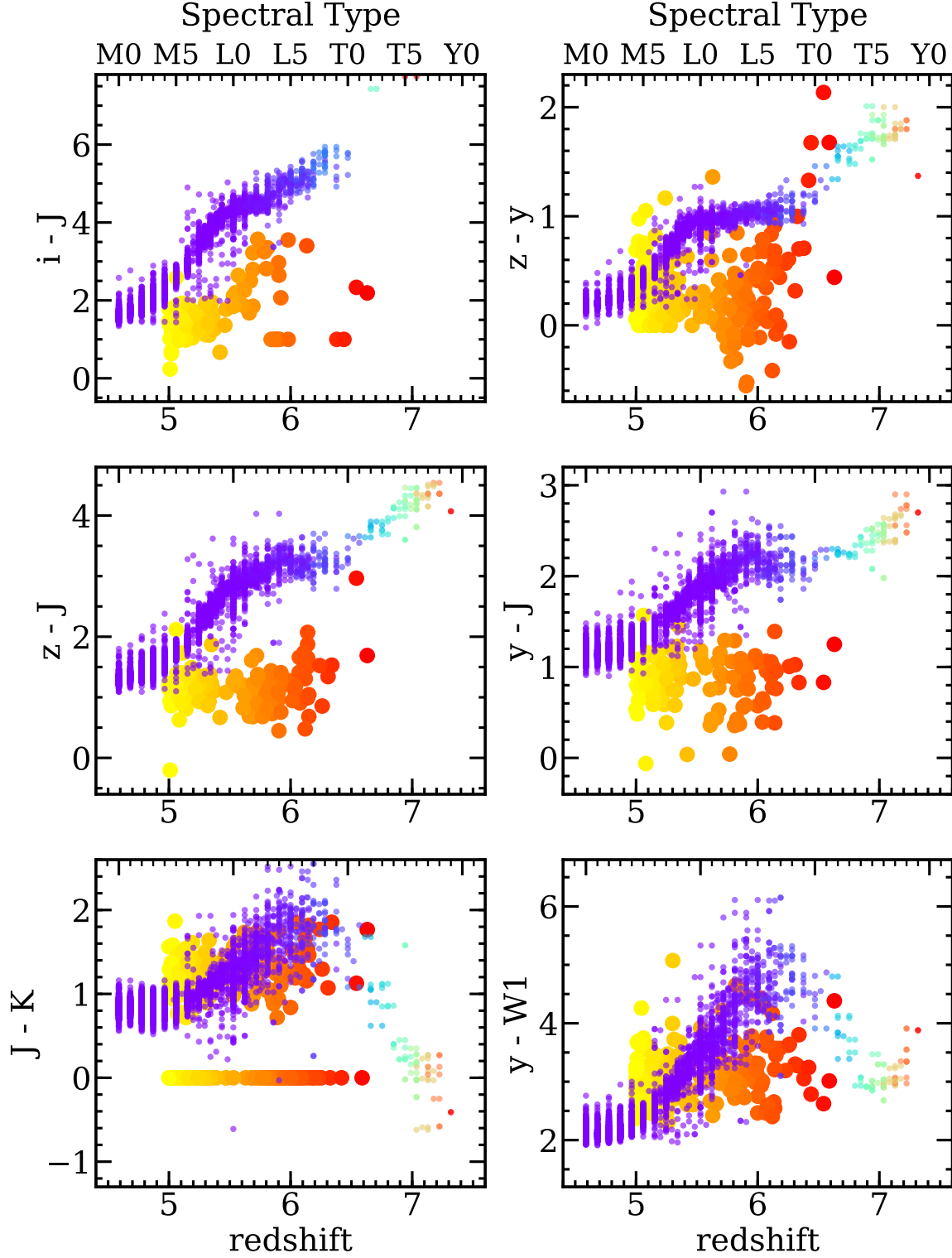
Figure 7. Optical colour vs. spectral type and redshift for Late Type M/L/T dwarfs and the VH*z*Qs. The stars are M, L, and T dwarfs from the Best et al. (2018) PS1-detected catalog. *N.B. Trying to look as good as Fig. 5 from Best et al. (2018). How does one get bigger gaps between subplots??*
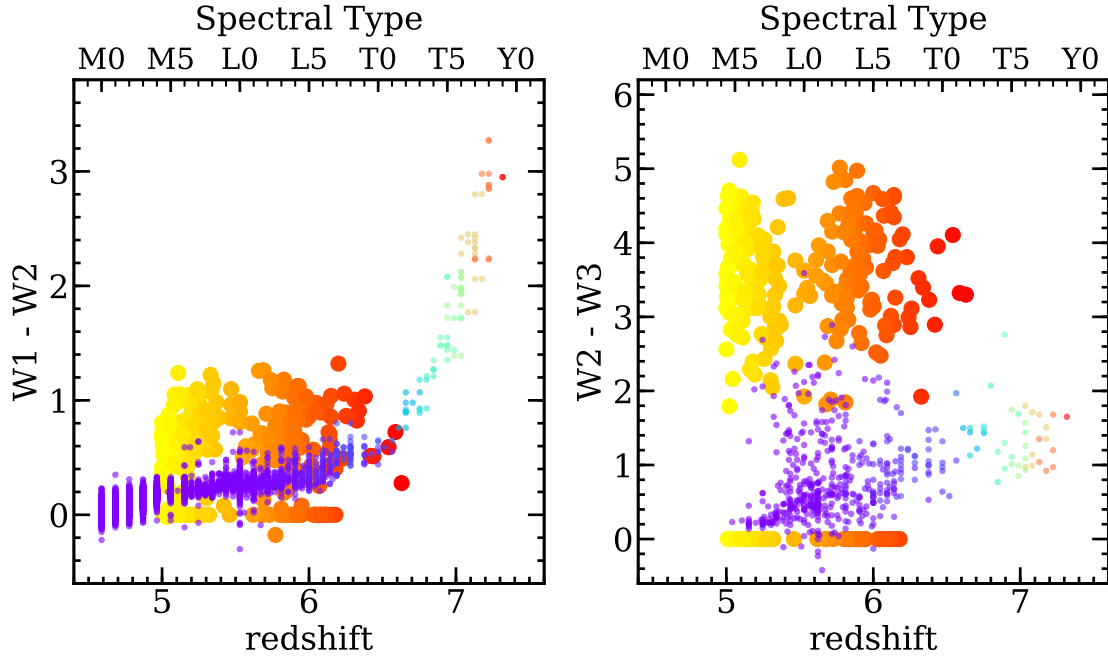
Figure 8. Infrared colour-spectral type and redshift plots for Late Type M/L/T dwarfs and the VHzQs. *NB* I'm really not sure how Best et al. actually get their stellar sequence so clean. There are two types of spectral classification, but restricting it to just SpT_optn or SpT_nir removes the blue or red end respectively. Hmmm....

Figure 9. Infrared colour-spectral type and redshift plots for Late Type M/L/T dwarfs and the VHzQs.

4   DISCUSSION AND CONCLUSIONS

In this study, we have, for the first time, ompiled the list of all $z > 5$ spectroscopically confirmed quasars. We have assemble the NIR ($y/Y, J, H, K/K_s$) and MIR (WISE W1/2/3/4) photometry for these objects, given their detection rates and SEDs. We find that:

We can gain a good appreciation for what these missions will discover by collating the datasets we currently have.

• Lorem ipsum dolor sit amet, consectetur adipiscing elit. Aliquam porta sodales est, vel cursus risus porta non. Vivamus vel pretium velit. Sed fringilla suscipit felis, nec iaculis lacus convallis ac.

• Fusce pellentesque condimentum dolor, quis vehicula tortor hendrerit sed. Class aptent taciti sociosqu ad litora torquent per conubia nostra, per inceptos himenaeos. Etiam interdum tristique diam eu blandit. Donec in lacinia libero.

• Sed elit massa, eleifend non sodales a, commodo ut felis. Sed id pretium felis. Vestibulum et turpis vitae quam aliquam convallis. Sed id ligula eu nulla ultrices tempus. Phasellus mattis erat quis metus dignissim malesuada. Nulla tincidunt quam volutpat nibh facilisis euismod. Cras vel auctor neque. Nam quis diam risus.

Nunc lacus nibh, convallis ac lobortis ut, tempus ac lectus. Maecenas eu elit massa. Nulla vel lacus lorem. Proin et lobortis tortor. Phasellus ultrices nisl non enim porttitor dictum. Curabitur nec nunc ac nibh ornare elementum. Nunc ultrices hendrerit ultricies. Aliquam dapibus semper est et gravida. Etiam cursus, massa eget tempor elementum, lectus urna feugiat nisi, eget sagittis.

Author Contributions

N.P.R. initiated the project, compiled the list of $z > 5.00$ quasars, wrote most of the analysis code, developed the the plotting scripts, and developed and wrote the initial and subsequent drafts of the manuscript. N.J.G.C. supplied the critical near-infrared expertise and database for which the bulk of the project relies. N.J.G.C. also contributed directly to the writing of the manuscript.

Availability of Data and computer analysis codes

All materials, databases, data tables and code are fully available at: https://github.com/d80b2t/VHzQ

Figure 10. The spectral bands used by different survey telescopes and that are relevant here.

[12] Rodrigo, C., Solano, E., Bayo, A. http://ivoa.net/documents/Notes/SVOFPS/index.html

Profile Service Access Protocol. Rodrigo, C., Solano, E. http://ivoa.net/documents/Notes/SVOFPSDAL/index.html

APPENDIX A: A. PHOTOMETRIC BANDS AND CONVERSIONS

Due to the differing normalizations between the SDSS and UKIDSS photometric systems, certain corrections are required. To present our data in the purest sense, all the NIR magnitudes from UKIDSS (originally AB magnitudes) were corrected to Vega magnitudes as suggested in Hewett et al. (2006).

Although ULAS magnitudes are reported in terms of Vega and SDSS magnitudes are reported in AB terms for the most part whenever an optical-NIR color was calculated both magnitudes were left in their default term.

https://www.gemini.edu/sciops/instruments/magnitudes-and-fluxes

APPENDIX B: PANSTARRS1 SQL QUERIES

The PS1 Casjobs SQL Server is located at mast-web.stsci.edu/ps1casjobs. The top level documentation is given here while the description of tables is given here. The main tables are the `objectThin` and `meanObject` tables.

Table A1. Adapted from Table 9 of González-Fernández et al. (2011). CTIO/DECam, PanSTARRS/PS1, LSST Filter only values. All wavelengths in Å. From González-Fernández et al. (2018) $Z_{AB} - Z_{Vega} = 0.502$; $Y_{AB} - Y_{Vega} = 0.600$; $J_{AB} - J_{Vega} = 0.916$; $H_{AB} - H_{Vega} = 1.366$; $Ks_{AB} - Ks_{Vega} = 1.827$; and the CASU Vega to AB conversions v1.3:: Z,Y,J,H,Ks were: 0.524, 0.618, 0.937, 1.384, 1.839. So, Δ(vs. Gonzalez-Fernandez):: (11.2, 1.1, 5.4, 1.6, 0.1) millimags. Δ(vsCASU v1.3):: (-10.8, -16.9, -15.6, -16.4, -11.9) millimags.

Band	λ_{eff}	λ_{min}	λ_{max}	W_{eff}	AB - Vega Transformations	
g_{HSC}	4633	3940	5546	1460	g_{HSC}	$= g_{\text{AB}} + 0.097$
g_{LSST}	4730	3877	5665	1333	g_{LSST}	$= g_{\text{AB}} + 0.083$
g_{DECam}	4734	3939	5528	1133	g_{DECam}	$= g_{\text{AB}} + 0.083$
g_{PS1}	4776	3943	5593	1167	g_{PS1}	$= g_{\text{AB}} + 0.080$
r_{HSC}	6104	5325	7071	1503	r_{HSC}	$= r_{\text{AB}} - 0.151$
r_{PS1}	6130	5386	7036	1318	r_{PS1}	$= r_{\text{AB}} - 0.153$
r_{LSST}	6139	5375	7055	1338	r_{LSST}	$= r_{\text{AB}} - 0.155$
r_{DECam}	6345	5506	7238	1379	r_{DECam}	$= r_{\text{AB}} - 0.192$
i_{PS1}	7485	6778	8304	1243	i_{PS1}	$= i_{\text{AB}} - 0.369$
i_{LSST}	7487	6765	8325	1209	i_{LSST}	$= i_{\text{AB}} - 0.369$
i_{HSC}	7633	6791	8658	1483	i_{PS1}	$= i_{\text{AB}} - 0.396$
i_{DECam}	7750	6950	8646	1371	i_{DECam}	$= i_{\text{AB}} - 0.415$
z_{PS1}	8658	8028	9346	966	z_{PS1}	$= z_{\text{AB}} - 0.508$
z_{LSST}	8669	8035	9375	994	z_{LSST}	$= z_{\text{AB}} - 0.509$
Z_{VIRCAM}	8762	8157	9400	978	Z_{VIRCAM}	$= Z_{\text{AB}} - 0.513$
Z_{WFCAM}	8802	8129	9457	926	Z_{WFCAM}	$= Z_{\text{AB}} - 0.514$
z_{HSC}	8915	8280	9498	793	Z_{HSC}	$= Z_{\text{AB}} - 0.512$
z_{DECam}	9216	8360	10166	1502	z_{DECam}	$= z_{\text{AB}} - 0.521$
y_{PS1}	9603	9100	10838	615	y_{PS1}	$= y_{\text{AB}} - 0.541$
y_{LSST}	9677	9089	10859	810	y_{LSST}	$= y_{\text{AB}} - 0.546$
Y_{DECam}	9876	9355	10730	676	Y_{DECam}	$= Y_{\text{AB}} - 0.570$
Y_{HSC}	9976	9000	10931	1386	Y_{HSC}	$= Y_{\text{AB}} - 0.580$
Y_{WFCAM}	10305	9790	10810	1020	Y_{WFCAM}	$= Y_{\text{AB}} - 0.617$
Y_{VIRCAM}	10184	9427	10977	905	Y_{VIRCAM}	$= Y_{\text{AB}} - 0.601$
J_{2MASS}	12350	10806	14068	1624	J_{2MASS}	$= J_{\text{AB}} - 0.894$
J_{VIRCAM}	12464	11427	13759	1628	J_{VIRCAM}	$= J_{\text{AB}} - 0.921$
J_{WFCAM}	12483	11690	13280	1590	J_{WFCAM}	$= J_{\text{AB}} - 0.919$
W_{Wircam}	14514	13890	15166	1020	W_{Wircam}	$= W_{\text{AB}} - 1.163$
H_{WFCAM}	16313	14920	17840	2920	H_{WFCAM}	$= H_{\text{AB}} - 1.379$
H_{VIRCAM}	16310	14604	18422	2833	H_{VIRCAM}	$= H_{\text{AB}} - 1.368$
H_{2MASS}	16620	14787	18231	2509	H_{2MASS}	$= H_{\text{AB}} - 1.374$
Ks_{VIRCAM}	21337	19333	23674	3055	Ks_{VIRCAM}	$= Ks_{\text{AB}} - 1.83$
Ks_{2MASS}	21590	19544	23552	2619	Ks_{2MASS}	$= Ks_{\text{AB}} - 1.84$
K_{WFCAM}	22010	20290	23800	3510	K_{WFCAM}	$= K_{\text{AB}} - 1.90$
WISE W1	33526	27541	38724	6626	W1	$= \text{W1}_{\text{AB}} - 2.699$
WISE W2	46028	39633	53414	10423	W2	$= \text{W2}_{\text{AB}} - 3.339$
WISE W3	115608	74430	172613	55056	W3	$= \text{W3}_{\text{AB}} - 5.174$
WISE W4	228172	195201	279107	41017	W4	$= \text{W4}_{\text{AB}} - 6.66$

```
1  SELECT s.ra, s.decl,
2          o.objID, o.raMean, o.decMean,
3          o.nDetections, o.ng, o.nr, o.ni, o.nz, o.ny,
4          m.gMeanPSFMag, m.gMeanPSFMagErr,  m.gMeanPSFMagStd,
5          m.rMeanPSFMag, m.rMeanPSFMagErr,  m.rMeanPSFMagStd,
6          m.iMeanPSFMag, m.iMeanPSFMagErr,  m.iMeanPSFMagStd,
7          m.zMeanPSFMag, m.zMeanPSFMagErr,  m.zMeanPSFMagStd,
8          m.yMeanPSFMag, m.yMeanPSFMagErr,  m.yMeanPSFMagStd,
9          s.jmag, s.jmag_error, s.hmag, s.hmag_error, s.kmag, s.kmag_error into mydb.MyTable_0 from M
10
```

```
11   cross apply fGetNearbyObjEq(s.ra,s.decl,2.0/60.0) nb
12   inner join ObjectThin o on o.objid=nb.objid and o.nDetections>1
13   inner join MeanObject m on o.objid=m.objid  and o.uniquePspsOBid=m.uniquePspsOBid
```

APPENDIX C: NEAR-INFRARED WFCAM SCIENCE ARCHIVE SQL QUERIES

Here we give the receipe and SQL that returned the near-infrared photometry for the VHzQs from the WFCAM Science Archive.

The data are on the WFCAM Science Archive: `wsa.roe.ac.uk`. Access the User Login form `wsa.roe.ac.uk/login.html` with these credentials::

- Username: `WSERV1000`
- password: `highzqso`
- community: `nonsurvey`

Then going to the `Free Form SQL Query` page the Database release `WSERV1000v20180716` can be accessed which contains all the data we use here.

We *nota bene* a few things. First, the quantity `aperJky3` and `aperJky3Err` are found in the `wserv1000MapRemeasAver` and `wserv1000MapRemeasurement`, so care has to be taken to return unique column names (otherwise e.g. astropy.io.fits will crash). As such, we alias `aver.aperJky3` to `aperJky3Aver` and likewise for the error quantity. Aliases will be necessary in some cases anyway, because some queries can be done sensibly on multiple instances of the same table. Other times, one may join tables on quantities such as `catalogueID` or `apertureID`, where you are meaning the same thing, but aliases would again be sensible.

Second, the `RA` and `DEC` values returned by the WSA are in radians, if used directly. To return values in degrees, use a selection with an alias, e.g. `RA as RADeg` and `DEC as DECDeg`.

Then the following SQL will return the values in Table 3.

```
1  SELECT
2  qso.qsoName,  qso.ra as raJ2000, qso.dec as decJ2000,
3  aver.apertureID,  aver.aperJky3 as aperJky3Aver,
4  aver.aperJky3Err as aperJky3AverErr, aver.sumWeight,
5  aver.ppErrBits as ppErrBitsAver, m.mjdObs,
6  m.filterID, remeas.aperJky3,
7  remeas.aperJky3Err,
8  w.weight, remeas.ppErrBits,
9  m.project
10
11 FROM
12 finalQsoCatalogue as qso,
13 MapApertureIDshighzQsoMap as ma,
14 wserv1000MapRemeasAver as aver,
15 wserv1000MapRemeasurement as remeas,
16 MapProvenance as v,
17 wserv1000MapAverageWeights as w,
18 MapFrameStatus as mfs,
19 Multiframe as m
20
21 WHERE
22 qso.qsoID=ma.objectID and
23 ma.apertureID=aver.apertureID and
24 aver.apertureID=remeas.apertureID and
25 aver.catalogueID=v.combicatID and
26 v.avSetupID=1 and
27 v.catalogueID=remeas.catalogueID and
28 w.combicatID=v.combicatID and
29 w.catalogueID=v.catalogueID and
30 w.apertureID=aver.apertureID and
31 mfs.catalogueID=remeas.catalogueID and
32 m.multiframeID=mfs.multiframeID and
33 mfs.programmeID=10999 and
34 mfs.mapID=1
35 order by v.combicatID, m.mjdObs
```

APPENDIX D: NEAR-INFRARED VISTA SCIENCE ARCHIVE SQL QUERIES

In a very similar manner to the WSA, we give here the details on how to access the VISTA Science Archive (VSA)

At the VSA Login, enter with these credentials::

- Username: `VSERV1000`
- password: `highzqso`
- community: `proprietary`

Then head to the Freeform SQL Query page where the database release to use is `VSERV1000v20180716`.

Then the following SQL will return the values in Table 3.

```
1  SELECT
2  qso.qsoName,  qso.ra as raJ2000, qso.dec as decJ2000,
3  aver.apertureID,  aver.aperJky3 as aperJky3Aver,
4  aver.aperJky3Err as aperJky3AverErr, aver.sumWeight,
5  aver.ppErrBits as ppErrBitsAver, m.mjdObs,
6  m.filterID, remeas.aperJky3,
7  remeas.aperJky3Err,
8  w.weight, remeas.ppErrBits,
9  m.project
10
11 FROM
12 finalQsoCatalogue as qso,
13 MapApertureIDshighzQsoMap as ma,
14 vserv1000MapRemeasAver as aver,
15 vserv1000MapRemeasurement as remeas,
16 MapProvenance as v,
17 vserv1000MapAverageWeights as w,
18 MapFrameStatus as mfs,
19 Multiframe as m
20
21 WHERE
22 qso.qsoID=ma.objectID and
23 ma.apertureID=aver.apertureID and
24 aver.apertureID=remeas.apertureID and
25 aver.catalogueID=v.combicatID and
26 v.avSetupID=1 and
27 v.catalogueID=remeas.catalogueID and
28 w.combicatID=v.combicatID and
29 w.catalogueID=v.catalogueID and
30 w.apertureID=aver.apertureID and
31 mfs.catalogueID=remeas.catalogueID and
32 m.multiframeID=mfs.multiframeID and
33 mfs.programmeID=10999 and
34 mfs.mapID=1
35 order by v.combicatID, m.mjdObs
```

REFERENCES

Agarwal B., Smith B., Glover S., Natarajan P., Khochfar S., 2016, MNRAS, 459, 4209

Alexander T., Natarajan P., 2014, Science, 345, 1330

Assef R. J., Stern D., Noirot G., Jun H. D., Cutri R. M., Eisenhardt P. R. M., 2018, ApJS, 234, 23

Astropy Collaboration et al., 2013, Astron. & Astrophys., 558, A33

Bañados E., et al., 2014, AJ, 148, 14

Bañados E., et al., 2016, ApJS, 227, 11

Bañados E., et al., 2018, Nat, 553, 473

Becker G. D., Bolton J. S., Lidz A., 2015, PASA, 32, 45

Becker R. H., White R. L., Helfand D. J., 1995, ApJ, 450, 559

Best W. M. J., et al., 2018, ApJS, 234, 1

Blain A., et al., 2013, ArXiv e-prints

Bosman S. E. I., et al., 2017, MNRAS, 470, 1919

Calura F., Gilli R., Vignali C., Pozzi F., Pipino A., Matteucci F., 2014, MNRAS, 438, 2765

Carilli C. L., et al., 2007, ApJ Lett., 666, L9

Carilli C. L., et al., 2010, ApJ, 714, 834

Carnall A. C., Shanks T., Chehade B., Fumagalli M., Rauch M., Irwin M. J., Gonzalez-Solares E., Findlay J. R., Metcalfe N., 2015, MNRAS, 451, L16

Casali M., et al., 2007, Astron. & Astrophys., 467, 777

Chambers K. C., et al., 2016, arXiv:1612.05560v3

Chen S.-F. S., et al., 2017, ApJ, 850, 188

Cool R. J., et al., 2006, AJ, 132, 823

Cross N., Hambly N., Collins R., Sutorius E., Read M., Blake R., 2013, in Adamson A., Davies J., Robson I., eds, Thirty Years of Astronomical Discovery with UKIRT Vol. 37 of Astrophysics and Space Science Proceedings, Discovery of Variables in WFCAM and VISTA Data. p. 193

Cross N. J. G., et al., 2012, Astron. & Astrophys., 548, A119

Cushing M. C., et al., 2006, ApJ, 648, 614

Cutri R. M. o., 2013, Technical report, Explanatory Supplement to the AllWISE Data Release Products

Dalton G. B., et al., 2006, in Society of Photo-Optical Instrumentation Engineers (SPIE) Conference Series Vol. 6269 of Proc. SPIE, The VISTA infrared camera. p. 62690X

De Rosa G., Decarli R., Walter F., Fan X., Jiang L., Kurk J., Pasquali A., Rix H. W., 2011, ApJ, 739, 56

Dey A., et al., 2018, ArXiv e-prints

Edge A., Sutherland W., Kuijken K., Driver S., McMahon R., Eales S., Emerson J. P., 2013, The Messenger, 154, 32

Emerson J., McPherson A., Sutherland W., 2006, The Messenger, 126, 41

Emerson J. P., Irwin M. J., Lewis J., Hodgkin S., Evans D., Bunclark P., McMahon R., Hambly N. C., Mann R. G., Bond I., Sutorius E., Read M., Williams P., Lawrence A., Stewart M., 2004, in P. J. Quinn & A. Bridger ed., Society of Photo-Optical Instrumentation Engineers (SPIE) Conference Series Vol. 5493 of Society of Photo-Optical Instrumentation Engineers (SPIE) Conference Series, VISTA data flow system: overview. pp 401–410

Fan X., 1999, AJ, 117, 2528

Fan X., Carilli C. L., Keating B., 2006, ARA&A, 44, 415

Fan X., et al., 2000, AJ, 119, 1

Fan X., et al., 2004, AJ, 128, 515

Fan X., et al., 2006, AJ, 132, 117

Fan X., et al., 2018, ArXiv e-prints

Fan X., Narayanan V. K., Lupton R. H., Strauss M. A., Knapp G. R., Becker R. H., White R. L., Pentericci L., et al., 2001, AJ, 122, 2833

Fan X., Strauss M. A., Schneider D. P., Becker R. H., White R. L., Haiman Z., Gregg M., Pentericci L., et al., 2003, AJ, 125, 1649

Flewelling H. A., et al., 2016, arXiv:1612.05243v2

Fukugita M., Ichikawa T., Gunn J. E., Doi M., Shimasaku K., Schneider D. P., 1996, AJ, 111, 1748

González-Fernández C., et al., 2018, MNRAS, 474, 5459

Goto T., 2006, MNRAS, 371, 769

Haardt F., Gorini V., Moschella U., Treves A., Colpi M., eds, 2016, Astrophysical Black Holes Vol. 905 of Lecture Notes in Physics, Berlin Springer Verlag

Hambly N. C., et al., 2008, MNRAS, 384, 637

Hewett P. C., Warren S. J., Leggett S. K., Hodgkin S. T., 2006, MNRAS, 367, 454

Hickox R. C., Myers A. D., Greene J. E., Hainline K. N., Zakamska N. L., DiPompeo M. A., 2017, ApJ, 849, 53

Hill A. R., Gallagher S. C., Deo R. P., Peeters E., Richards G. T., 2014, MNRAS, 438, 2317

Ikeda H., Nagao T., Matsuoka K., Kawakatu N., Kajisawa M., Akiyama M., Miyaji T., Morokuma T., 2017, ApJ, 846, 57

Jannuzi B. T., Dey A., 1999, in Weymann R., et al. eds, ASP Conf. Ser. 191: Photometric Redshifts and the Detection of High Redshift Galaxies p. 111

Jiang L., et al., 2006, AJ, 132, 2127

Jiang L., et al., 2008, AJ, 135, 1057

Jiang L., et al., 2009, AJ, 138, 305

Jiang L., et al., 2010, Nat, 464, 380

Jiang L., McGreer I. D., Fan X., Bian F., Cai Z., Clément B., Wang R., Fan Z., 2015, AJ, 149, 188

Kaiser N., et al., 2002, in J. A. Tyson & S. Wolff ed., Society of Photo-Optical Instrumentation Engineers (SPIE) Vol. 4836, Pan-STARRS: A Large Synoptic Survey Telescope Array. pp 154–164

Kaiser N., et al., 2010, in Society of Photo-Optical Instrumentation Engineers (SPIE) Vol. 7733, The Pan-STARRS wide-field optical/NIR imaging survey. p. 0

Kashikawa N., Ishizaki Y., Willott C. J., Onoue M., Im M., Furusawa H., Toshikawa J., Ishikawa S., Niino Y., Shimasaku K., Ouchi M., Hibon P., 2015, ApJ, 798, 28

Kim Y., et al., 2015, ApJ Lett., 813, L35

Kim Y., et al., 2018, ArXiv e-prints

Koptelova E., Hwang C.-Y., Yu P.-C., Chen W.-P., Guo J.-K., 2017, Scientific Reports, 7, 41617

Kurk J. D., et al., 2007, ApJ, 669, 32

Kurk J. D., Walter F., Fan X., Jiang L., Jester S., Rix H.-W., Riechers D. A., 2009, ApJ, 702, 833

Lacy M., et al., 2004, ApJS, 154, 166

Lang D., 2014, AJ, 147, 108

Lang D., Hogg D. W., Jester S., Rix H., 2009, AJ, 137, 4400

Latif M. A., Volonteri M., Wise J. H., 2018, arXiv:1801.07685v1

Lawrence A., et al., 2007, MNRAS, 379, 1599

Le Fèvre O., et al., 2003, in Iye M., Moorwood A. F. M., eds, Instrument Design and Performance for Optical/Infrared Ground-based Telescopes Vol. 4841 of Proc. SPIE, Commissioning and performances of the VLT-VIMOS instrument. pp 1670–1681

Leipski C., et al., 2014, ApJ, 785, 154

Lupi A., Haardt F., Dotti M., Fiacconi D., Mayer L., Madau P., 2016, MNRAS, 456, 2993

Madau P., Haardt F., Dotti M., 2014, ApJ Lett., 784, L38

Magnier E. A., et al., 2016a, arXiv:1612.05242v2

Magnier E. A., et al., 2016b, arXiv:1612.05244v2

Magnier E. A., et al., 2016c, arXiv:1612.05240v2

Mahabal A., Stern D., Bogosavljević M., Djorgovski S. G., Thompson D., 2005, ApJ Lett., 634, L9

Mainzer A., et al., 2011, ApJ, 731, 53

Mainzer A., et al., 2014, ApJ, 792, 30

Matsuoka Y., et al., 2016, ApJ, 828, 26

Matsuoka Y., et al., 2018a, PASJ, 70, S35

Matsuoka Y., et al., 2018b, ApJS, 237, 5

Mazzucchelli C., et al., 2017, ApJ, 849, 91

McGreer I. D., Becker R. H., Helfand D. J., White R. L., 2006, ApJ, 652, 157

McGreer I. D., et al., 2013, ApJ, 768, 105

Meisner A. M., Lang D., Schlegel D. J., 2018a, Research Notes of the American Astronomical Society, 2, 1

Meisner A. M., Lang D. A., Schlegel D. J., 2018b, Research Notes of the American Astronomical Society, 2, 202

Miyazaki S., et al., 2018, PASJ, 70, S1

Morganson E., et al., 2012, AJ, 143, 142

Mortlock D., 2016, in Mesinger A., ed., Understanding the Epoch of Cosmic Reionization: Challenges and Progress Vol. 423 of Astrophysics and Space Science Library, Quasars as Probes of Cosmological Reionization. p. 187

Mortlock D. J., et al., 2009, Astron. & Astrophys., 505, 97

Mortlock D. J., et al., 2011, Nat, 474, 616

Mortlock D. J., Patel M., Warren S. J., Hewett P. C., Venemans B. P., McMahon R. G., Simpson C., 2012, MNRAS, 419, 390

Oke J. B., Gunn J. E., 1983, ApJ, 266, 713

Peth M. A., Ross N. P., Schneider D. P., 2011, AJ, 141, 105

Pezzulli E., Valiante R., Schneider R., 2016, MNRAS, 458, 3047

Pezzulli E., Volonteri M., Schneider R., Valiante R., 2017, MNRAS, 471, 589

Reed S. L., et al., 2015, MNRAS, 454, 3952

Reed S. L., et al., 2017, MNRAS, 468, 4702

Rees M. J., 1984, ARA&A, 22, 471

Richards G. T., et al., 2006, ApJS, 166, 470

Ross N. P., et al., 2013, ApJ, 773, 14

Sawicki M., 2002, AJ, 124, 3050

Schlafly E. F., Meisner A. M., 2018, ApJS

Shanks T., et al., 2015, MNRAS, 451, 4238

Simcoe R. A., Sullivan P. W., Cooksey K. L., Kao M. M., Matejek M. S., Burgasser A. J., 2012, Nat, 492, 79

Stern D., et al., 2005, ApJ, 631, 163

Stern D., et al., 2007, ApJ, 663, 677

Stoughton C., et al., 2002, AJ, 123, 485

Takeo E., Inayoshi K., Ohsuga K., Takahashi H. R., Mineshige S., 2018, MNRAS, 476, 673

Tang J.-J., et al., 2017, MNRAS, 466, 4568

Taylor M., , 2011, TOPCAT: Tool for OPerations on Catalogues And Tables, Astrophysics Source Code Library

Taylor M. B., 2005, in Shopbell P., Britton M., Ebert R., eds, Astronomical Data Analysis Software and Systems XIV Vol. 347 of Astronomical Society of the Pacific Conference Series, TOPCAT & STIL: Starlink Table/VOTable Processing Software. p. 29

The Astropy Collaboration et al., 2018, ArXiv e-prints

Tielens A. G. G. M., 2008, ARA&A, 46, 289

Timlin J. D., Ross N. P., et al., 2016, ApJS, 225, 1

Väisänen P., Tollestrup E. V., Willner S. P., Cohen M., 2000, ApJ, 540, 593

Valiante R., Schneider R., Graziani L., Zappacosta L., 2018, MNRAS, 474, 3825

Vanden Berk D. E., et al., 2001, AJ, 122, 549

Venemans B. P., et al., 2012, ApJ Lett., 751, L25

Venemans B. P., et al., 2013, ApJ, 779, 24

Venemans B. P., et al., 2015a, MNRAS, 453, 2259

Venemans B. P., et al., 2015b, ApJ Lett., 801, L11

Venemans B. P., McMahon R. G., Warren S. J., Gonzalez-Solares E. A., Hewett P. C., Mortlock D. J., Dye S., Sharp R. G., 2007, MNRAS, 376, L76

Venemans B. P., Walter F., Zschaechner L., Decarli R., De Rosa G., Findlay J. R., McMahon R. G., Sutherland W. J., 2016, ApJ, 816, 37

Volonteri M., 2010, A&ARv, 18, 279

Volonteri M., Silk J., Dubus G., 2015, ApJ, 804, 148

Wang F., et al., 2016, ApJ, 819, 24

Wang F., et al., 2017, ApJ, 839, 27

Wang F., et al., 2018a, arXiv:1810.11926v1

Wang F., et al., 2018b, arXiv:1810.11925v1

Wang R., et al., 2008, ApJ, 687, 848

Wang R., et al., 2011, ApJ Lett., 739, L34

Waters C. Z., et al., 2016, arXiv:1612.05245v4

Willott C. J., Bergeron J., Omont A., 2015, ApJ, 801, 123

Willott C. J., et al., 2007, AJ, 134, 2435

Willott C. J., et al., 2009, AJ, 137, 3541

Willott C. J., et al., 2010, AJ, 139, 906

Willott C. J., Omont A., Bergeron J., 2013, ApJ, 770, 13

Wise J. H., Regan J. A., O'Shea B. W., Norman M. L., Downes T. P., Xu H., 2019, arXiv:1901.07563v1

Wright E. L., Eisenhardt P. E., Fazio G. G., 1994, ArXiv Astrophysics e-prints

Wright E. L., et al., 2010, AJ, 140, 1868

Wu X.-B., et al., 2015, Nat, 518, 512

Wyithe J. S. B., Loeb A., 2003, ApJ, 586, 693

Yan L., Sajina A., Fadda D., Choi P., Armus L., Helou G., Teplitz H., Frayer D., Surace J., 2007, ApJ, 658, 778

Yang J., et al., 2017, AJ, 153, 184

Yang J., et al., 2018a, arXiv:1811.11915v1

Yang J., et al., 2018b, arXiv:1810.11927v1

Zeimann G. R., White R. L., Becker R. H., Hodge J. A., Stanford S. A., Richards G. T., 2011, ApJ, 736, 57